
This is an electronic reprint of the original article.
This reprint may differ from the original in pagination and typographic detail.

Jokinen, Miikka; Manzanares Andreu, Jose; Kontturi, Kyösti; Murtomäki, Lasse
Thermal potential of ion-exchange membranes and its application to thermoelectric power generation

Published in:
Journal of Membrane Science

DOI:
[10.1016/j.memsci.2015.10.042](https://doi.org/10.1016/j.memsci.2015.10.042)

Published: 01/02/2016

Document Version
Peer-reviewed accepted author manuscript, also known as Final accepted manuscript or Post-print

Please cite the original version:
Jokinen, M., Manzanares Andreu, J., Kontturi, K., & Murtomäki, L. (2016). Thermal potential of ion-exchange membranes and its application to thermoelectric power generation. *Journal of Membrane Science*, 499, 234-244. <https://doi.org/10.1016/j.memsci.2015.10.042>

This material is protected by copyright and other intellectual property rights, and duplication or sale of all or part of any of the repository collections is not permitted, except that material may be duplicated by you for your research use or educational purposes in electronic or print form. You must obtain permission for any other use. Electronic or print copies may not be offered, whether for sale or otherwise to anyone who is not an authorised user.

Thermal potential of ion-exchange membranes and its application to thermoelectric power generation

Miikka Jokinen^a, José A. Manzanares^{a,b}, Kyösti Kontturi^{a,†}, Lasse Murtomäki^{a,}*

a Department of Chemistry, School of Chemical Technology, Aalto University, P.O. Box 16100, FI-00076 Aalto, Finland.

b Department of Thermodynamics, Faculty of Physics, University of Valencia, E-46100 Burjassot, Spain

Keywords: thermal membrane potential, ion-exchange membranes, thermoelectric power generation, non-isothermal electrodiffusion, ionic Seebeck coefficient, ionic heat of transport

ABSTRACT

The low efficiency and high price of thermoelectric semiconductors has generated interest in unconventional forms of thermoelectric materials. In this article, ionic thermoelectricity has been studied with commercial ion-exchange membranes for different aqueous 1:1 electrolytes. The theory of thermal membrane potential has been derived taking into account the ionic heats of transport, the non-isothermal Donnan potentials, the temperature polarization, and the thermally-induced concentration polarization of the electrolyte. Also the generated thermoelectric power has

been experimentally studied. The experiments show good agreement with the theory, and suggest ways for systematic improvement of the system performance.

1. Introduction

Thermoelectric materials have been subject to intense research, especially over the past 15 years [1,2]. They offer a means for converting thermal energy directly into electricity [3-5], with a myriad of potential applications from small scale space applications to large scale geothermal power production and heat harvesting [1,3]. However, the poor efficiency and high price of the materials are still hindering commercialization [2,3]. The problems with existing thermoelectric materials and their stagnating development have diverted interest towards other forms of thermoelectricity, with promising results [2,5,6].

Ion-exchange membranes have been previously suggested as an alternative to semiconductors in terms of thermoelectricity [7]. A temperature difference ΔT over a charged membrane in electrolyte solution creates an electric potential difference $\Delta\phi$, known as the thermal membrane potential [8,9]. The Seebeck coefficients of membrane systems are similar or larger than that of semiconductor thermoelectric materials [4,10]. This can be partly attributed to the typically three orders of magnitude difference in the heats of transport of ions and electrons [8,11], and partly to the Donnan potential difference created by the temperature difference over the membrane [12]. Moreover, polymer membranes have relatively low thermal conductivity [7], a desired property for a thermoelectric material [1,2,4]. Lower fabrication costs associated with polymer membranes, with respect to semiconductor materials, form another advantage [7].

Previous studies of the thermal membrane potential have considered the effects of the electrolyte and its concentration [10,13-17], the thermal polarization [18], the mean temperature [19], and the

hydrophobicity of the ion-exchange groups [20]. The combination of thermal membrane potential and streaming potential has also been studied [7]. Reports on the thermal membrane potential for common chloride electrolytes, such as LiCl, KCl, NaCl, and HCl, can be found in the literature, but there are discrepancies with the magnitude of their Seebeck coefficients. Barragán and Ruiz-Bauzá reported a descending order for the Seebeck coefficient as $\text{LiCl} > \text{NaCl} > \text{KCl}$ with a cation-exchange membrane, and attributed this order to increasing molar mass of the cations [18]. Hanaoka *et al.* [17] obtained a descending order $\text{KCl} > \text{LiCl} \approx \text{NaCl} > \text{HCl}$ for the Seebeck coefficients with cation-exchange membranes in the concentration range 1–100 mmol/L, and highlighted a similar trend for the inverse of the crystallographic radius of the cations. Few authors [8] have tried to explain the thermal membrane potential with ionic transport quantities, especially heats of transport. The heat of transport *Q_i is defined as the heat transferred by one mole of species i through a reference plane in the absence of temperature gradient [11] and is widely used in the study of thermodiffusion in electrolyte solutions. Experimental data for these transport quantities can be readily found in the literature [11,21,22] and they can be useful in the evaluation of the thermal membrane potential.

The purpose of this study is to investigate thermoelectric power generation using ion-exchange membranes, which has not been experimentally studied before. The influence of several experimentally relevant parameters on the electrical power generation is analyzed. Our theoretical modeling of the thermal membrane potential takes into account the thermal polarization effect [18], the concentration dependence of the heats of transport, and the concentration polarization thermally-induced by the Soret effect [23].

The structure of the article is as follows. Section 2 shows the theory of the thermal membrane potential. Section 3 briefly describes the experimental methods. In Section 4 we first provide the

measurements of thermal membrane potential with a range of 1:1 electrolytes at different concentrations and then analyze the thermoelectric power output as a function of temperature difference, concentration, and number of modules. The article ends with a discussion section.

2. Theory

2.1 Description of the system

The experimental cell under study has four narrow compartments with solutions of the same 1:1 electrolyte and concentration (Figure 1). All solutions are pumped through the cell to large vessels, which provides mixing and maintains the desired temperature and composition. The temperature of one of the solutions, referred to as the "hot" solution, is varied while the other three solutions have fixed temperature. The electrode compartments are separated by means of anion-exchange membranes and a cation-exchange membrane separates the hot solution from the cold one. Thus, temperature gradients exist across the cation-exchange and one of the anion-exchange membranes (Figure 1). Under open-circuit conditions, these temperature gradients drive electrolyte and (thermo-osmotic) water transport through the two membranes. The strongly-charged nature of the membranes creates electric potential drops across them, which add to give the thermally-generated open-circuit cell potential. These potential drops have contributions from the (Donnan) equilibrium distribution at the membrane-solution interfaces and from the thermal electrodiffusion of ions both inside the membrane and in the external solutions. However, when strongly-charged membranes are used, the major contribution to the thermal membrane potential arises from the temperature dependence of the Donnan potentials, as the electrolyte diffusion through the membranes is practically negligible. In other words, even though the system is not under equilibrium conditions when temperature gradients exist, the low permeability of the

membranes for co-ions and the absence of electric current (open-circuit conditions) render the ionic flux densities very small.

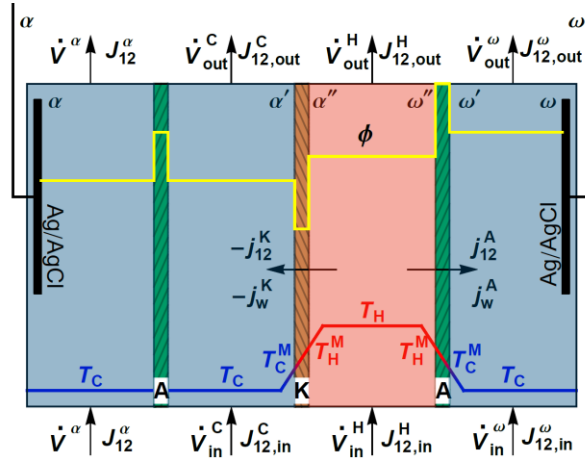


Figure 1. Diagram of the (single-module) experimental setup. H and C stand for hot and cold solutions, A and K for anion- and cation-exchange membrane, and α and ω for the electrode compartments. The solutions in all compartments are circulated. The inlet and outlet flow rates are \dot{V}_{in} and \dot{V}_{out} , respectively. The inlet and outlet electrolyte fluxes are $J_{12,in} = c_{12,in}\dot{V}_{in}$ and $J_{12,out} = c_{12,out}\dot{V}_{out}$. The temperature and electrostatic potential distributions are indicated.

When Ag/AgCl electrodes are used, the cell potential is $\phi^\omega - \phi^\alpha = -(\tilde{\mu}_-^\omega - \tilde{\mu}_-^\alpha)/F$ where ω denotes the electrode closer to the hot solution and α the other one, $\tilde{\mu}_-$ is the (molar) electrochemical potential of the chloride ions and F is Faraday's constant. This potential difference can be approximated by $\phi^\omega - \phi^\alpha \approx (\phi^{\alpha''} - \phi^{\alpha'}) + (\phi^{\omega'} - \phi^{\omega''}) \approx \Delta\phi^K + \Delta\phi^A$, where the positions ω'' , ω' , α'' and α' are indicated in Figure 1, because the homogeneity of both temperature and electrolyte concentration implies $\phi^\omega \approx \phi^{\omega'}$, $\phi^\alpha \approx \phi^{\alpha'}$ and $\phi^{\omega''} \approx \phi^{\alpha''}$.

In the following subsections we describe the transport of ions and energy in the direction normal to the membranes, where x is taken as positive from α to ω . Firstly, we consider one membrane extending from $x = 0$ to $x = h$ flanked by boundary layers of thickness δ . The concentration and temperature at $x = -\delta$ are identified by a superscript α , and those at $x = h + \delta$ by a superscript β , although superscript α has also been used for the left electrode. Secondly, the membrane system of Figure 1 is considered by adding the contributions from the anion- and cation-exchange membranes.

2.2 Temperature polarization

Even though the solutions are well stirred, layers with temperature gradients exist on both sides of the membranes adjacent to the hot solution. This effect is known as temperature polarization [24] and must be taken into account when determining the thermal membrane potential [18,25,26]. While heat transport inside the membrane is conductive, heat is transferred by a combination of conduction and convection in the polarization layers [18].

The reduced heat flux density inside the membrane is [11,27]

$$j_q = -\lambda^M \frac{dT}{dx} + {}^*Q_1^M j_1 + {}^*Q_2^M j_2 \quad (1)$$

where ${}^*Q_i^M$ is the heat of transport of ionic species i ($i = 1, 2$), and λ^M is the static thermal conductivity of the membrane. The ionic contributions to j_q are negligible (even at the short-circuit current of a thermocell) and the steady-state heat flux density can be simply described as $j_q = -P_T^M [T(h) - T(0)]$, where P_T^M is the thermal permeability of the membrane [18]. Similarly, in the thermally-polarized boundary layers of thickness δ flanking the membrane, the reduced

heat flux density can be described as $j_q = -P_T^w \Delta T^\delta$, where $\Delta T^\delta = T^\beta - T(h) = T(0) - T^\alpha$ and P_T^w is the thermal permeability (or heat transfer coefficient) that takes into account the conduction and convection mechanisms [18]. The temperatures of the bulk solutions are $T(-\delta) = T^\alpha$ and $T(h + \delta) = T^\beta = T^\alpha + \Delta T$.

Under steady-state conditions, the continuity of the heat flux density requires that $P_T^M \Delta T^M = P_T^w \Delta T^\delta$. Thus, the temperature drop inside the membrane

$$\Delta T^M \equiv T(h) - T(0) = \Delta T / (1 + 2P_T^M / P_T^w) \equiv k \Delta T \quad (2)$$

is a fraction $k < 1$ of the applied temperature difference. Making reference to the symbols introduced in Figure 1, eq 2 can also be presented as $T_H^M - T_C^M = k(T_H - T_C)$.

2.3 Interfacial Donnan equilibria

The local electroneutrality condition inside a membrane with uniform molar concentration X of fixed charge groups is

$$c_1^M(x) = c_2^M(x) + X \quad (3)$$

where counterions and co-ions are identified by subscripts 1 and 2, respectively [28]. The external solutions at the boundaries $x = 0$ and $x = h$ have, in general, different temperature $T(x)$ and electrolyte molar concentration, $c_1^w = c_2^w = c(x)$. From the condition of ionic distribution equilibrium at the membrane boundaries, the Donnan interfacial potential drops $\Delta\phi_D(0) = \phi^M(0) - \phi^w(0)$ and $\Delta\phi_D(h) = \phi^M(h) - \phi^w(h)$ are given by

$$\frac{z_2 F \Delta\phi_D(x)}{RT(x)} = \operatorname{arcsinh} \frac{X}{2c(x)}, \quad (x = 0, h) \quad (4)$$

where R is the gas constant and z_i is the charge number of ionic species i [28]. Their difference can be expressed as

$$\frac{z_2 F}{R \bar{T}} [\Delta \phi_D(0) - \Delta \phi_D(h)] \approx \tanh \varphi_D \frac{c(h) - c(0)}{\bar{c}} - \varphi_D \frac{T(h) - T(0)}{\bar{T}}, \quad (5)$$

where $\bar{c} \equiv [c(0) + c(h)]/2$, $\bar{T} \equiv [T(0) + T(h)]/2$, and $\varphi_D \equiv \operatorname{arcsinh} X / 2\bar{c}$. The first term in the rhs of eq 5 is the contribution from the concentration difference and the second term the contribution from the temperature difference at the external membrane boundaries. In the cation-exchange membrane ($z_2 = -1$), the latter contribution is

$$\Delta \phi_D^K = \varphi_D^K \frac{R}{F} (T_H^M - T_C^M). \quad (6)$$

and, similarly, in the thermally-polarized anion-exchange membrane it is

$$\Delta \phi_D^A = \varphi_D^A \frac{R}{F} (T_H^M - T_C^M). \quad (7)$$

These two are major and additive contributions to the measured open-circuit potential $\Delta \phi_{oc}$. These expressions clearly show a linear dependence on the temperature drop across the membranes, as well as the typical order of magnitude of $\Delta \phi_{oc} / \Delta T$, i.e. the Seebeck coefficient of the membrane cell, which is dictated by $R/F = 86.17 \mu\text{V/K}$. Using strongly-charged membranes ($X \gg c$), this coefficient can be increased by one order of magnitude thanks to the prefactor φ_D in eqs 5 and 6. (The Seebeck coefficient of semiconductors is also of the order of R/F , while that of metals is typically lower by a factor T/T_F , where T_F is the Fermi temperature of the metal.) Thus, the theoretical prediction is that the thermal membrane potential should decrease with increasing electrolyte concentration, as determined by $\varphi_D \equiv \operatorname{arcsinh}(X/2c)$.

2.4 Electric potential drop inside the membrane

Within the Nernst-Planck approximation, the molar flux density of ionic species i ($i=1,2$) inside the membrane is [11]

$$j_i = -\frac{t_i^M \sigma^M}{F^2} \left({}^*Q_i^M \frac{d \ln T}{dx} + RT \frac{d \ln c_i^M}{dx} + z_i F \frac{d \phi^M}{dx} \right) \quad (8)$$

where $t_i^M(x) = (D_i^M c_i^M) / (D_1^M c_1^M + D_2^M c_2^M)$ is the migrational transport number of species i and $\sigma^M(x) = (F^2 / RT)(D_1^M c_1^M + D_2^M c_2^M)$ is the electrical conductivity of the membrane. The effect of thermo-osmosis [29] on the ionic flux density is neglected. Substituting eq 8 in the expression $d\phi_{\text{ohm}} / dx \equiv -I / \sigma^M = -F(z_1 j_1 + z_2 j_2) / \sigma^M$ for the Ohmic potential gradient, the gradient of the electrostatic potential inside the membrane is

$$\frac{d\phi^M}{dx} = \frac{d\phi_{\text{th}}}{dx} + \frac{d\phi_{\text{dif}}}{dx} + \frac{d\phi_{\text{ohm}}}{dx} \quad (9)$$

where

$$\frac{d\phi_{\text{dif}}}{dx} \equiv -\frac{RT}{z_2 F} \frac{D_2^M - D_1^M}{D_1^M c_1^M + D_2^M c_2^M} \frac{dc_2^M}{dx} \quad (10)$$

is the gradient of the diffusion potential,

$$\frac{d\phi_{\text{th}}}{dx} \equiv -\Pi^M \frac{d \ln T}{dx} \quad (11)$$

is the gradient of the thermal diffusion potential, and $\Pi^M = (t_1^M {}^*Q_1^M - t_2^M {}^*Q_2^M) / (z_2 F)$ is the ionic Peltier coefficient.

The integration of these gradients across the membrane yields

$$\Delta\phi_{\text{ohm}}^M \approx -\frac{RT}{F^2} \frac{Ih}{D_1^M X + (D_2^M + D_1^M)\bar{c}_2^M} \quad (12)$$

$$\Delta\phi_{\text{dif}}^{\text{M}} = -\frac{R\bar{T}}{z_2F} \frac{D_2^{\text{M}} - D_1^{\text{M}}}{D_1^{\text{M}}X + (D_2^{\text{M}} + D_1^{\text{M}})\bar{c}_2^{\text{M}}} [c_2^{\text{M}}(h) - c_2^{\text{M}}(0)] \quad (13)$$

$$\Delta\phi_{\text{th}}^{\text{M}} \approx \frac{\bar{t}_1^{\text{M}} * \bar{Q}_1^{\text{M}} - \bar{t}_2^{\text{M}} * \bar{Q}_2^{\text{M}}}{z_2F} \ln \frac{T(h)}{T(0)} \quad (14)$$

where \bar{t}_i^{M} and $*\bar{Q}_i^{\text{M}} = *Q_i^{\text{M}}(\bar{T})$ are the migrational transport number and the heat of transport of species i corresponding to the average temperature $\bar{T} \equiv [T(0) + T(h)]/2 \approx (T_{\text{H}} + T_{\text{C}})/2$ and average concentration inside the membrane; this result takes into account a typical temperature dependence of the ionic heat of transport, $*\bar{Q}_i^{\text{M}}(T) = AT^2 - B$ where A and B are coefficients [11]. Obviously, eq 12 is only relevant under closed-circuit conditions and eq 13 yields a negligible contribution in strongly charged membranes separating two solutions of identical concentration.

The average co-ion transport number inside the membrane satisfies the equation

$$\frac{1}{\bar{t}_2^{\text{M}}} = 1 + \frac{D_1^{\text{M}}\bar{c}_1^{\text{M}}}{D_2^{\text{M}}\bar{c}_2^{\text{M}}} = 1 + \frac{D_1^{\text{M}}}{D_2^{\text{M}}} \exp(2\phi_{\text{D}}) \quad (15)$$

and can be neglected at low electrolyte concentrations $\bar{c} \ll X$ [28]. In that case, eq 14 simplifies to $z_2F\Delta\phi_{\text{th}}^{\text{M}} \approx *\bar{Q}_1^{\text{M}} \ln[T(h)/T(0)] \approx (*\bar{Q}_1^{\text{M}}/\bar{T})[T(h) - T(0)]$. The physical meaning of this potential drop inside the membrane can be explained with the help of eq 8. Since the counterion flux density is almost zero under open-circuit conditions and the concentration gradient inside the membrane is also negligible, eq 8 for the counterion reduces to $*Q_1^{\text{M}}d\ln T + z_1F d\phi^{\text{M}} = 0$. If $*Q_i^{\text{M}} > 0$, this ion would tend to go towards positions of lower temperature. Since it cannot move under open-circuit conditions, an electric field builds inside the membrane so that the positions of lower temperature are also those of higher electrostatic energy for the counterions, and the counterion tendency to flow is thus cancelled.

The contribution of the thermal diffusion potentials to the cell potential in Figure 1 is

$$\Delta\phi_{\text{th}}^{\text{K}} + \Delta\phi_{\text{th}}^{\text{A}} \approx -\frac{*\bar{Q}_+^{\text{K}} + *\bar{Q}_-^{\text{A}}}{F\bar{T}}(T_{\text{H}}^{\text{M}} - T_{\text{C}}^{\text{M}}) \approx -\frac{*\bar{Q}_+^{\text{K}} + *\bar{Q}_-^{\text{A}}}{FT_{\text{C}}}(T_{\text{H}}^{\text{M}} - T_{\text{C}}^{\text{M}}) \quad (16)$$

where $*\bar{Q}_+^{\text{K}}$ is the heat of transport of the cations in the cation-exchange membrane and $*\bar{Q}_-^{\text{A}}$ the heat of transport of the anions in the anion-exchange membrane. The first approximation in eq 16 is accurate to the second order in $(T_{\text{H}}^{\text{M}} - T_{\text{C}}^{\text{M}})/\bar{T}$ while the second approximation is accurate only to the first order. Thus, while both can be used for small temperature gradients, the former should be preferred for larger gradients. Equation 16 clearly shows that the effect of the thermal diffusion of the counterions is to decrease the Seebeck coefficient $\Delta\phi_{\text{oc}}/\Delta T$ of the membrane cell by a quantity $(*\bar{Q}_+^{\text{K}} + *\bar{Q}_-^{\text{A}})/(FT_{\text{C}})$.

2.5 Thermal diffusion potentials in the boundary layers

Equation 2 implies that temperature drops $\Delta T^{\delta} = (1-k)\Delta T/2$ exist in each boundary layer, which generate thermal diffusion potential gradients described by equations similar to eq 11. The integration of these gradients across the boundary layers yields

$$\Delta\phi_{\text{th}}^{\alpha} = \phi_{\text{th}}(0) - \phi_{\text{th}}(-\delta) \approx \frac{\bar{t}_1^{\alpha} *\bar{Q}_1^{\alpha} - \bar{t}_2^{\alpha} *\bar{Q}_2^{\alpha}}{z_2 F} \ln \frac{T(0)}{T^{\alpha}} \approx \frac{\bar{t}_1^{\alpha} *\bar{Q}_1^{\alpha} - \bar{t}_2^{\alpha} *\bar{Q}_2^{\alpha}}{z_2 FT^{\alpha}} \Delta T^{\delta} \quad (17)$$

$$\Delta\phi_{\text{th}}^{\beta} = \phi_{\text{th}}(h+\delta) - \phi_{\text{th}}(h) \approx \frac{\bar{t}_1^{\beta} *\bar{Q}_1^{\beta} - \bar{t}_2^{\beta} *\bar{Q}_2^{\beta}}{z_2 F} \ln \frac{T^{\beta}}{T(h)} \approx \frac{\bar{t}_1^{\beta} *\bar{Q}_1^{\beta} - \bar{t}_2^{\beta} *\bar{Q}_2^{\beta}}{z_2 FT^{\beta}} \Delta T^{\delta} \quad (18)$$

where the overbar denotes the average value over the layer. Introducing the approximations

$\bar{t}_i^{\alpha} \approx \bar{t}_i^{\beta} \approx t_i^{\text{w}} = D_i^{\text{w}}/(D_1^{\text{w}} + D_2^{\text{w}})$ and $*\bar{Q}_i^{\alpha} \approx *\bar{Q}_i^{\beta} \approx *Q_i^{\text{w}}$, the sum of these potential drops is

$$\Delta\phi_{\text{th}}^{\text{w}} \equiv \Delta\phi_{\text{th}}^{\alpha} + \Delta\phi_{\text{th}}^{\beta} \approx \frac{t_1^{\text{w}} *Q_1^{\text{w}} - t_2^{\text{w}} *Q_2^{\text{w}}}{z_2 F} \frac{T^{\alpha} + T^{\beta}}{T^{\alpha} T^{\beta}} \Delta T^{\delta}. \quad (19)$$

Taking into account the temperature gradients across the cation- and anion-exchange membranes (see Figure 1), these terms are

$$\Delta\phi_{\text{th}}^{\text{w,K}} \approx -\frac{t_+^{\text{w}*}Q_+^{\text{w}} - t_-^{\text{w}*}Q_-^{\text{w}}}{F} \frac{T_{\text{H}} + T_{\text{C}}}{T_{\text{H}}T_{\text{C}}} \frac{1-k}{2} (T_{\text{H}} - T_{\text{C}}) \quad (20)$$

$$\Delta\phi_{\text{th}}^{\text{w,A}} \approx \frac{t_+^{\text{w}*}Q_+^{\text{w}} - t_-^{\text{w}*}Q_-^{\text{w}}}{F} \frac{T_{\text{H}} + T_{\text{C}}}{T_{\text{H}}T_{\text{C}}} \frac{1-k}{2} (T_{\text{H}} - T_{\text{C}}) \quad (21)$$

and cancel each other. The reason for the cancellation is clear from eq 19. Subscripts 1 and 2 denote the counterions and co-ions, respectively. The first fraction in the rhs of eq 19 does not change sign when considering the cation- or the anion-exchange membrane (because both numerator and denominator reverse sign), but the temperature gradients (and, hence, ΔT^{δ}) in these membranes have opposite signs; note that the characteristics of these membranes are so similar, except for the sign of the fixed charge, that the temperature gradients across them only differ in sign.

2.6 Thermal concentration polarization and diffusion potential drops

Even though the electrolyte solutions have the same electrolyte concentration $c = c^{\alpha} = c(-\delta) = c(h + \delta) = c^{\beta}$, the concentrations $c(0)$ and $c(h)$ at the external membrane boundaries may differ from each other because the temperature gradients in the boundary layers may induce thermal diffusion of the electrolyte. However, the actual extent of this thermal concentration polarization is difficult to quantify. Should the solutions be stagnant, because they were not circulated and the gravitational convection were somehow eliminated, the Soret distribution equilibrium would be achieved and the electrolyte concentrations at the membrane

boundaries, $c(0)$ and $c(h)$, would be different from the concentrations $c^\alpha = c^\beta = c$ of the bulk solutions. The Soret distribution equilibrium equations are

$$\frac{c(0)}{c} = \exp \left\{ \frac{*\bar{Q}_{12}^\alpha}{2R} \left[\frac{1}{T(0)} - \frac{1}{T^\alpha} \right] \right\} \approx 1 - \frac{*\bar{Q}_{12}^w}{2RT^\alpha} \frac{\Delta T^\delta}{T^\alpha} \quad (22)$$

$$\frac{c(h)}{c} = \exp \left\{ \frac{*\bar{Q}_{12}^\beta}{2R} \left[\frac{1}{T(h)} - \frac{1}{T^\beta} \right] \right\} \approx 1 + \frac{*\bar{Q}_{12}^w}{2RT^\beta} \frac{\Delta T^\delta}{T^\beta} \quad (23)$$

where $*\bar{Q}_{12}^w = *\bar{Q}_1^w + *\bar{Q}_2^w$ is the heat of transport of the electrolyte (at the average temperature and concentration of the boundary layer). Thus, for the usual case $*\bar{Q}_{12}^w > 0$, the electrolyte would accumulate at the external membrane boundary facing the hot solution, and be depleted from the external membrane boundary facing the cold solution.

Should these concentration gradients exist, the first term in the rhs of eq 5 describing the contribution from the thermal concentration polarization to the Donnan potentials might be relevant. From eqs 22 and 23, it is possible to estimate that the difference in the electrolyte concentrations between the two external membrane boundaries as $c(h) - c(0) \approx [*\bar{Q}_{12}^w c / R(T_C)^2] \Delta T^\delta$. If $*\bar{Q}_{12}^w > 0$, this difference has the same sign as ΔT^δ , and hence it is positive for the cation-exchange membrane and negative for the anion-exchange membrane (see Figure 1). Thus, the thermal concentration polarization (tcp) contributions to the cell potential from the cation- and anion-exchange membranes are additive and can be estimated from eq 5 as

$$\Delta \phi_{\text{tcp}} \approx -\frac{*\bar{Q}_{12}^w}{FT_C} (1-k)(T_H - T_C) \quad (24)$$

where the approximation $\tanh \phi_D \approx 1$, valid for strongly charged membranes [11], has been used.

It is important to notice, however, that in our experimental setup the solutions are circulated (with a relatively high flow rate) and it is rather unlikely that the Soret distribution equilibria of eqs 22 and 23 are actually established, for they are easily perturbed by any convective motion. In this case, eq 24 would not be a contribution to the cell potential. Although we were inclined to believe that this is actually the case, the possible influence of the contribution in eq 24 will be considered in the analysis of the experimental data.

It could be thought, at first, that the concentration gradients also bring a contribution to the cell potential from the diffusion potentials. The diffusion potentials inside the membranes are negligible because the co-ion concentration gradients (see eq 13) are negligible in strongly charged membranes [11]. Assuming that the solutions are stagnant and, hence, that eqs 22 and 23 apply, the diffusion potential drop in the boundary layers of one membrane are

$$\Delta\phi_{\text{dif}}^{\alpha} = \phi_{\text{dif}}(0) - \phi_{\text{dif}}(-\delta) = -\frac{RT^{\alpha}}{z_2F} (t_2^w - t_1^w) \ln \frac{c(0)}{c^{\alpha}} \approx (t_2^w - t_1^w) \frac{Q_{12}^w}{2z_2F} \frac{\Delta T^{\delta}}{T^{\alpha}} \quad (25)$$

$$\Delta\phi_{\text{dif}}^{\beta} = \phi_{\text{dif}}(h + \delta) - \phi_{\text{dif}}(h) = -\frac{RT^{\beta}}{z_2F} (t_2^w - t_1^w) \ln \frac{c^{\beta}}{c(h)} \approx (t_2^w - t_1^w) \frac{Q_{12}^w}{2z_2F} \frac{\Delta T^{\delta}}{T^{\beta}} . \quad (26)$$

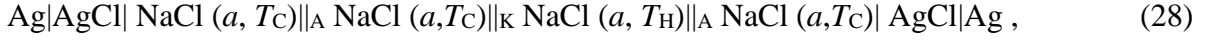
However, as was also the case for the thermal diffusion potentials in eqs 20 and 21, their effects cancel out because

$$\Delta\phi_{\text{dif}}^{\text{K}} = \Delta\phi_{\text{dif}}^{\alpha,\text{K}} + \Delta\phi_{\text{dif}}^{\beta,\text{K}} \approx (t_+^w - t_-^w) \frac{Q_{12}^w}{F} \frac{1-k}{2} \frac{T_{\text{H}} - T_{\text{C}}}{T_{\text{H}}} = -\Delta\phi_{\text{dif}}^{\text{A}} . \quad (27)$$

The reason for the cancellation is that the thermal diffusion of the electrolyte in the hot solution induces two regions with opposite concentration gradients, one close to the cation- and the other close to the anion-exchange membrane; the concentration gradients at the other boundaries of these membranes also have opposite signs and, hence, compensating effects.

2.7 Thermal potential of a cell combining cation- and anion-exchange membranes

In the cell



where a is the activity, the potential drops are associated with the membranes separating solutions at different temperature. The e.m.f. $\Delta\phi_{oc} = \Delta\phi_D^K + \Delta\phi_D^A + \Delta\phi_{th}^K + \Delta\phi_{th}^A + \Delta\phi_{tcp}$ of this cell, from eqs 2, 6, 7, 16, and 24, is

$$\Delta\phi_{oc} \approx \left[k(\phi_D^K + \phi_D^A) \frac{R}{F} - \frac{k(*\bar{Q}_+^K + *\bar{Q}_-^A) + (1-k)*Q_{12}^w}{FT_C} \right] (T_H - T_C). \quad (29)$$

Since the heat of transport depends strongly on the concentration [11], $*\bar{Q}_i^M$ and $*\bar{Q}_i^w$ may be significantly different. Yet, the comparison of eq 29 with experimental data would not yield separate values of $*\bar{Q}_i^M$ and $*\bar{Q}_i^w$ but only a value for the whole second fraction inside brackets.

Similarly, instead of trying to determine separately X^K and X^A , we can introduce an average fixed charge concentration $X \equiv (X^A X^K)^{1/2}$ and approximate $\phi_D^K + \phi_D^A \approx 2 \operatorname{arcsinh}(X/2c)$. Thus, a simplified theoretical equation that can be used to analyze the experimental observations is

$$\Delta\phi_{oc} \approx \left[k \frac{2R}{F} \operatorname{arcsinh} \frac{X}{2c} - \beta \frac{*Q_{12}^w}{FT_C} \right] (T_H - T_C) \quad (30)$$

where k and β are parameters to be determined, and X can be estimated from transport number measurements (and from the manufacturer information). The quantity inside brackets in eq 30, $\Delta\phi_{oc} / \Delta T$, is the Seebeck coefficient of the membrane cell.

3. Experimental Methods

3.1 Electrodes

For all electrodes, two pieces of silver wire (99.9%, 1 mm in thickness) were cut and polished with SiC-paper. The electrodes were rinsed with deionized water (Merck Millipore, USA) and acetone (Fisher Scientific, 99.9%), after which they were placed in an ultrasonic bath in a 0.10 mol/L HCl solution (Merck) for 10 minutes. After the ultrasonic treatment, the electrodes were again rinsed with water and acetone. The silver wires were short circuited with a large surface area Pt-electrode in 0.10 mol/L HCl (for Ag/AgCl-electrodes) or in 0.10 mol/L KI (> 99%, Sigma-Aldrich, for Ag/AgI-electrodes), and the respective silver halide was left to form onto the silver wire overnight. The following day, the electrodes were connected to a potentiostat (Metrohm Autolab PGSTAT12, the Netherlands) and cyclic voltammetry was run between -1 V and 1 V for 4000 cycles with a sweep rate of 0.25 V/s. This method produced pairs of electrodes with a stable and small potential difference.

3.2 The cell

The basic setup had four narrow compartments connected by apertures of 0.496 cm² and 4 mm in thickness with solutions of the same electrolyte and concentration (Figure 1). The electrolytes were $\geq 99\%$ purity from Sigma-Aldrich, except for tetramethylammonium chloride (TMACl, 99% Fluka). The solutions in the four compartments were pumped through the cell to large vessels, to provide mixing and maintain the desired temperature and composition. A cation-exchange membrane (Dupont Nafion 117) separated the hot and cold solutions. The electrode compartments were separated from them using anion-exchange membranes (Fumatech Fumapem FAA-3). The temperatures were measured with calibrated K-type thermocouples. The temperature of the

electrode compartments was kept at 298.2 K, as was the cold compartment, while that of the “hot” compartment was varied. Before each measurement, the membranes were equilibrated with the electrolyte solutions. Each thermal membrane potential was measured several times so that any drift could be observed and corrected. The sign convention is such that a positive thermal potential indicates that the electrode next to the hot solution is positive with respect to the other electrode.

3.3 Power output

In order to determine the thermally-generated electrical power, the potential drop was measured over a variable resistor (Danbridge, Denmark) connected in series with the thermoelectric cell. The current was calculated from Ohm’s law and the resistance was gradually decreased from 100 k Ω . When the external resistance is much larger than the cell resistance, the potential drop in the former is, to a good approximation, the open-circuit cell e.m.f. (or thermal membrane potential).

3.4 Thermal conductivity

The thermal conductivity λ^M of the wet ion-exchange membranes was measured in-plane with a TCi Thermal Conductivity Analyzer (C-Therm Technologies, Canada) at various temperatures over a stack of 25 membranes. The stack was used as the individual membrane samples were too thin for reliable analysis. To minimize the contact resistance between the samples, a weight of 1 kg was used to compress the sensor against the membranes.

4. Results

4.1 Counterion transport number

At the concentration of 0.02 mol/L used in most of our thermal membrane potential measurements, the counterion transport number is expected to be close to unity, especially in the Nafion membranes. Yet, hydrogen ions might leak as co-ions in anion-exchange membranes. The counterion transport number has been determined as $t_- = 1 + \Delta\phi_{\text{cell}}/2\ln(a_{\text{R}}/a_{\text{L}})$, where $a_{\text{R}} \equiv \gamma_{\text{R}}c_{\text{R}}$ and $a_{\text{L}} \equiv \gamma_{\text{L}}c_{\text{L}}$ are the electrolyte activities in the solutions and γ is the activity coefficient. The values measured at 0.02 mol/L (Figure 2) are sufficiently close to unity so that the membranes can be considered as ideally permselective in relation to the experimental determination of the thermal membrane potential. Further analysis (see Supporting information) shows that the fixed charge concentration of the membrane was $X \approx 3$ mol/L, a reasonable value for commercial ion-exchange membranes [30].

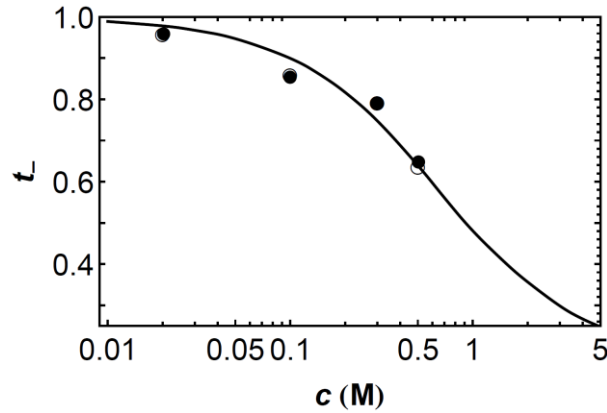


Figure 2. Potentiometric transport number of the chloride ion in the anion-exchange FAA-3 membrane immersed in HCl solutions at 25 °C, with $c_{\text{L}} = 0.5c$ and $c_{\text{R}} = 1.5c$. The open symbols have no activity coefficient correction and the full symbols are corrected measurements. The theoretical curve corresponds to $X = 3.0$ mol/L and $D_{\text{HCl}}^{\text{M}}\delta/D_{\text{HCl}}d = 0.3$, where $D_{\text{HCl}}^{\text{M}}$ and D_{HCl} are the diffusion coefficients in the membrane and the external solutions, respectively, d is the

membrane thickness and δ the boundary layer thickness. The diffusion coefficients in the external solutions are $D_{\text{H}^+}^{\text{w}} = 9.31 \times 10^{-5} \text{ cm}^2/\text{s}$ and $D_{\text{Cl}^-}^{\text{w}} = 2.03 \times 10^{-5} \text{ cm}^2/\text{s}$ [31]; and the high concentration limit is $t_-^{\text{w}} = D_{\text{Cl}^-}^{\text{w}} / (D_{\text{Cl}^-}^{\text{w}} + D_{\text{H}^+}^{\text{w}})$.

4.2 Thermal membrane potential and its concentration dependence

Equation 30 predicts that the open-circuit potential of the thermocell is proportional to the temperature difference ΔT_{M} between the two membrane boundaries, which is a fraction k of the temperature difference ΔT between the external electrolyte solutions, $\Delta T_{\text{M}} = k \Delta T$. The proportionality coefficient between the quantities $\Delta \phi_{\text{oc}}$ and ΔT is the Seebeck coefficient of the membrane cell. The experimental results confirm this theoretical prediction.

The inset in Figure 3a shows an example of the measured thermal membrane potentials in 0.10 mol/L NaCl for ΔT ranging between -7 and 20 K. Although the heat of transport term in eq 30 is negative, the dominating Donnan term makes the slope positive. In the measurements, $T_{\text{C}} = 298.2$ K is kept constant and T_{H} is varied. Although this is a routine procedure, it has sometimes been advised to vary both T_{C} and T_{H} while keeping constant their average value [19]. For the relatively small temperature differences here employed, both procedures are valid since no deviations from linear behavior are observed.

The Seebeck coefficient $\Delta \phi_{\text{oc}} / \Delta T$ decreases with increasing electrolyte concentration (Figure 3a). The concentration dependence of the thermal membrane potential mainly arises from the Donnan potential contributions. That is, the term proportional to $\text{arcsinh}(X/2c) \approx \ln(X/c)$ in eq 30 dominates. To illustrate this fact, eq 30 for ${}^*Q_{12}^{\text{w}} = 0$, $X = 3.0$ mol/L and $k = 1/4$ has been

plotted as a dashed line, and qualitative agreement with the measurements for KCl and NaCl is observed (Figure 3a). The differences between the Seebeck coefficients of the membrane systems with these two electrolytes are explained when the electrolyte heat of transport is taken into account. The Seebeck coefficient is larger for the electrolyte with smaller heat of transport (KCl). The quantitative agreement between the theoretical prediction of eq 30 with an estimated electrolyte heat of transport and the experimental observations is not perfect but quite satisfactory, especially when realizing that the heat of transport varies with concentration and that the values reported by different authors show significant dispersion.

Figures 3b and 3c show the Soret coefficients of KCl and NaCl at 25 °C as a function of the square root of their molar concentration. Smooth trend lines similar to those in Fig. 5 of Ref. [32] have been drawn. Neglecting the activity correction, the relation between the Soret coefficient s_T of the electrolyte and its heat of transport is ${}^*Q_{12}^w = 2RT^2 s_T$ [11]. Incorporating the experimental heats of transport of these electrolytes (Figures 3b and 3c) yields a better agreement between our experimental data and the theoretical prediction (eq 30). The parameter β in eq 30 is then estimated as $\beta = 0.6 \pm 0.3$ for KCl and $\beta = 0.89 \pm 0.16$ for NaCl, where the relatively large uncertainties indicate that the thermally-generated potential is not very sensitive to ${}^*Q_{12}^w$. These values of β are reasonable taking into account that the state of the ions (especially their concentration) inside the membranes differs from that in the external solutions and, hence, the approximation ${}^*Q_i^M \approx {}^*Q_i^w$ introduces a significant uncertainty. To obtain these values of β in eq 30, the fixed charge concentration X and the factor k describing the fraction of the temperature drop residing inside the membrane have been fixed to the estimated values $X = 3.0$ mol/L (see Figure 2) and $k = 1/3$. The thermal conductivity of water at 300 K is $0.6 \text{ W m}^{-1} \text{ K}^{-1}$ [33], and the

value measured for the membranes was $\lambda_{\text{Nafion}}^{\text{M}} \approx \lambda_{\text{FAA-3}}^{\text{M}} \approx 0.25 \text{ W m}^{-1} \text{ K}^{-1}$, similar to the value reported elsewhere for Nafion [34]. This suggests that the thickness of the temperature polarization region is of the same order than the membrane thickness, thus yielding the estimation $k \approx 1/3$.

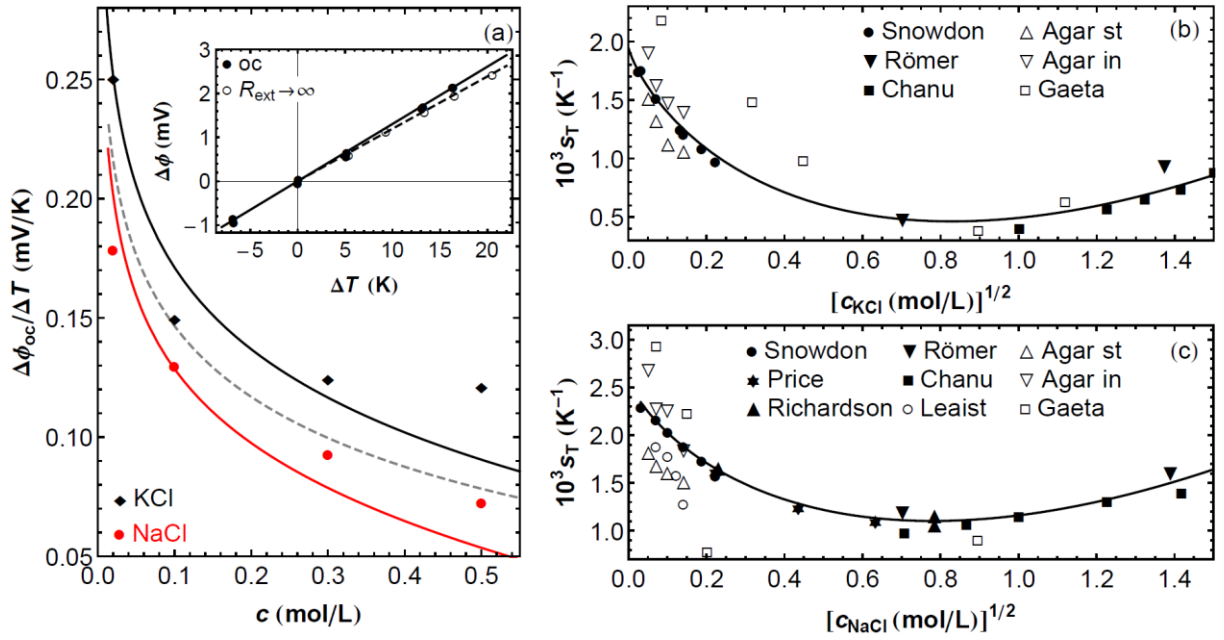


Figure 3. (a) Variation of the Seebeck coefficient of the membrane cell with NaCl and KCl concentration. The solid lines represent eq 30 with the electrolyte heats of transport estimated from the trend lines in panels (b) and (c), $X = 3$ mol/L and $k = 1/3$ fixed, and β as the only fitting parameter ($\beta = 0.6 \pm 0.3$ for KCl and 0.89 ± 0.16 for NaCl). The dashed line corresponds to $Q_{12}^w = 0$, $X = 3$ mol/L, and $k = 1/4$. The inset shows the potential difference measured in 0.10 mol/L NaCl. The full symbols are open-circuit measurements (slope 0.131 mV/K) and the open symbols are extrapolations of the closed-circuit measurements in the limit of infinite external load (slope 0.120 mV/K). (b and c) Concentration dependence of the Soret coefficient of NaCl and KCl aqueous solutions at 25 °C. The symbols are experimental data from the literature:

Snowdon [21], Price [35], Römer [36], Chanu [37], Leaist [38], Agar st (steady-state values) and Agar in (initial values) [39], and Gaeta [40] (data corresponding to 30 °C).

4.3 Influence of the electrolyte on the thermal membrane potential

As different ions have different heats of transport, different electrolytes generate different thermal membrane potentials. In order to confirm the theoretical predictions, the thermal membrane potentials of a selection of 1:1 chloride and iodide electrolytes in 0.02 mol/L concentration were measured. To the best of our knowledge, there are no measurements of electrolyte heats of transport in ion-exchange membranes in the literature. Although the different state of the ions inside the membrane pores and in the external solutions is likely to imply changes in the ionic heats of transport, some correlation between the heats of transport inside the membrane and in the external solutions could be expected [8]. Hence, the heats of transport of the electrolytes at 25 °C and 0.02 mol/L must be compiled from the literature. These have been presented in Table 1. Some values have been measured at the correct concentration, and some have been estimated from the relations derived by Snowdon and Turner for 1:1 electrolytes: ${}^*Q_{12}^w(0.02\text{ mol/kg}) \approx {}^*Q_{12}^w(0\text{ mol/kg}) - 1.48\text{ kJ/mol} \approx {}^*Q_{12}^w(0.01\text{ mol/kg}) - 0.43\text{ kJ/mol}$ [21].

Table I. Heats of transport of electrolytes at 0.02 mol/L and 25 °C.

	${}^*Q_i^w$ (kJ/mol)	Ref.
LiCl	-0.42 [†]	[23,41-43]
LiI	-2.5 [†]	[23,41,42]
TMACl	9.1 [†]	[44]
NaCl	2.66	[21]
KCl	1.70	[21]

KI	-0.34	[21]
HCl	12.45	[45]

†Estimated from the reference values at infinite dilution and 0.01 mol/L and the relations reported in Ref. [21].

Figure 4 shows that the Seebeck coefficient $\Delta\phi_{oc}/\Delta T$ of the membrane thermocell presents a linear correlation with the electrolyte heat of transport in the external solution ${}^*Q_{12}^w$, as theoretically predicted by eq 30. However, the two electrolytes with potassium ions deviate from this correlation. Because some approximations have been used to derive this equation, some deviation is to be expected. The fact that only potassium ions seem to deviate from the theoretical prediction might indicate that their state inside the membrane, in relation to the transport of energy, is different to that of the other cations under consideration. We have commented above that the heats of transport of KI, LiI and LiCl are negative at 25 °C and 0.02 mol/L. Alexander [46], Gaeta et al. [40], and Römer et al. [36] have reported sign inversions in the Soret coefficient of KCl, NaCl and LiCl upon decreasing the electrolyte concentration in solution [40,47]; although other results did not support some of these observations [48]. Moreover, the heat of transport of KCl exhibits quite a strong temperature dependence [36]. Although the actual origin of the deviation observed in Figure 4 for KCl and KI is unknown, the peculiarities of the dependence of the heats of transport of these electrolytes with temperature, concentration and ionic hydration seem to be relevant.

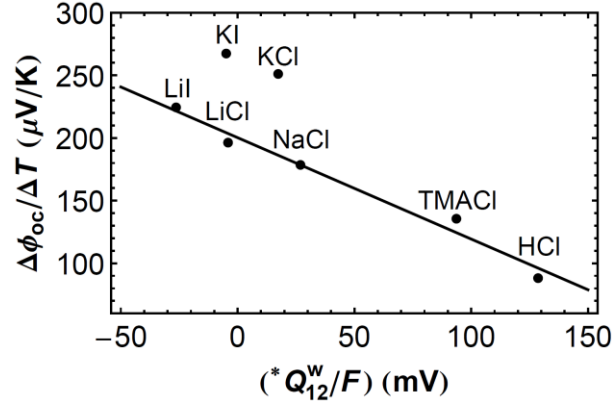


Figure 4. The Seebeck coefficients $\Delta\phi_{oc}/\Delta T$ measured for different electrolytes show a linear correlation with the electrolyte heat of transport in the external solution $*Q_{12}^w$ at 0.02 mol/L and $T_C = 298.2$ K. The two electrolytes with potassium ions deviate from this correlation, however.

4.4 Electrical power output

The measured cell potential is the sum of the thermal membrane potential, proportional to the temperature difference $\Delta T_M = k\Delta T$ between the membrane boundaries, and a contribution from the electrodes. The latter can be determined from the plot of the measured cell potential vs. ΔT as the intercept at the origin, $\Delta\phi_{cell} = \Delta\phi + (\Delta\phi)_{\Delta T=0}$.

When the cell is connected to an external electrical resistance R_{ext} the thermally-generated potential drives electrons in the external circuit and ions in the ion-exchange membranes so that electrical current and power is delivered (Figure 5). The thermal membrane potential is then $\Delta\phi = \Delta\phi_{oc} R_{ext} / (R_{ext} + R_{int})$ where $\Delta\phi_{oc}$ is the e.m.f. or open-circuit cell potential and R_{int} is the internal cell resistance. The experimental characteristic curves of thermal potential $\Delta\phi$ versus current I are linear, which indicates that R_{int} is independent of the current and $\Delta\phi = \Delta\phi_{oc} - IR_{int}$.

The electrical output power $P = I\Delta\phi = (\Delta\phi_{oc})^2 R_{ext} / (R_{ext} + R_{int})^2$ takes its maximum value P_{max}

when the variable external load is set equal to the internal cell resistance, $R_{\text{ext}} = R_{\text{int}}$. For a given temperature difference, electrolyte concentration, and number of modules, five sets of experimental data ($\Delta\phi$ vs. R_{ext} , i vs. R_{ext} , P/A vs. R_{ext} , $\Delta\phi$ vs. i , and P/A vs. i) are fitted to the above equations using $\Delta\phi_{\text{oc}}$ and R_{int} as fitting parameters that take the same values in the five sets. The open-circuit potentials $\Delta\phi_{\text{oc}}$ in Figures 6-8 have been obtained using this procedure.

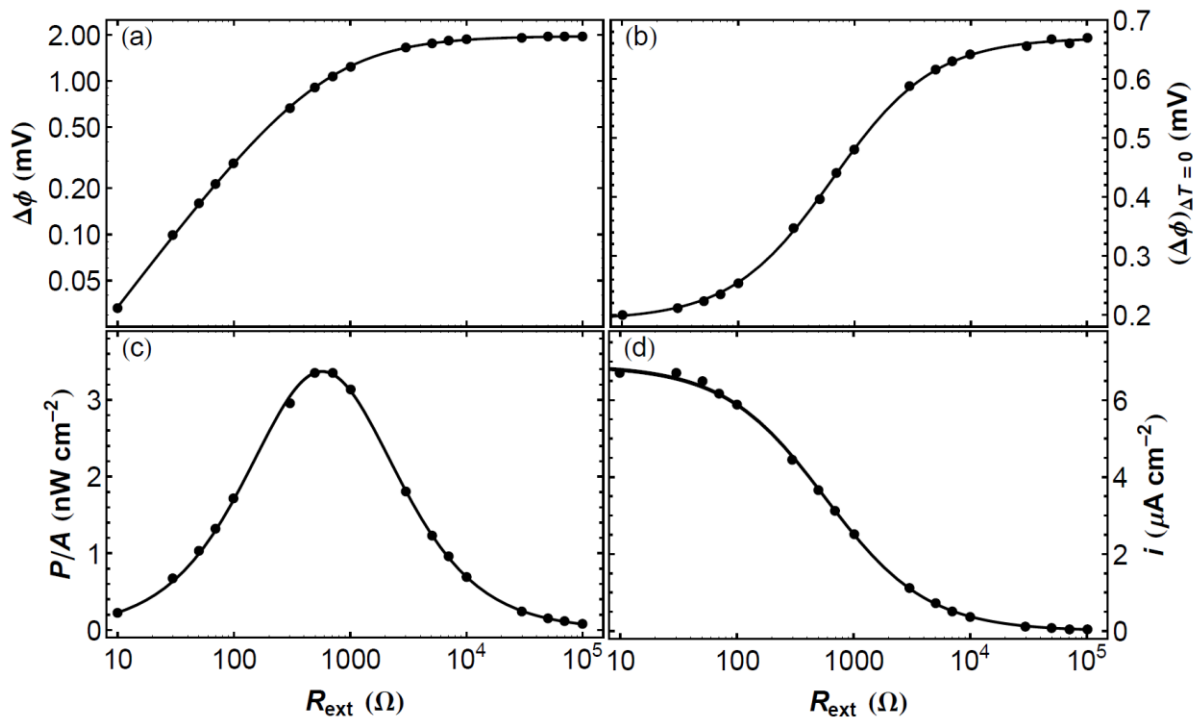


Figure 5. The cell potential $\Delta\phi_{\text{cell}}$ is the sum of the thermal membrane potential $\Delta\phi$ and a contribution from the asymmetry of the electrode potentials $(\Delta\phi)_{\Delta T=0}$. The experimental data presented here correspond to 0.10 mol/L NaCl and $\Delta T = 16.5\text{K}$. The cell potential decreases and the current delivered by the cell increases when the external load R_{ext} connected to the cell decreases. Thus, the electrical power output exhibits a maximum when R_{ext} is equal to the internal

electrical resistance of the cell R_{int} . Thus, it is determined that $R_{\text{int}} = 574 \Omega$ and $P_{\text{max}} / A = 3.38 \text{ nW/cm}^2$. The current density is $i = I/A = \Delta\phi / (AR_{\text{ext}})$ where $A = 0.496 \text{ cm}^2$ is the exposed membrane area. The open-circuit thermal membrane potential is $(\Delta\phi)_{\text{oc}} = 1.96 \text{ mV}$.

The experimental characteristic curves $\Delta\phi$ vs. i are linear (Figure 6a), and follow the expected behavior $\Delta\phi = \Delta\phi_{\text{oc}} - IR_{\text{int}}$. Figure 6a also shows that, for a fixed electrolyte concentration (0.10 mol/L NaCl), the internal electrical resistance of the cell is practically independent of the temperature difference. The electrical output power also shows the expected dependence with the delivered current, $P = I^2 R_{\text{ext}} = I(I_{\text{sc}} - I)R_{\text{int}}$, where $I_{\text{sc}} = \Delta\phi_{\text{oc}} / R_{\text{int}}$ is the short-circuit current delivered by the cell. Figures 6a and 6c show that the open-circuit potential and the output current through the external load increase as ΔT increases from 5.36 K to 20.53 K, resulting in an increase of the maximum power generation from 0.33 nW/cm² for $\Delta T = 5.36 \text{ K}$ to 5.14 nW/cm² for $\Delta T = 20.53 \text{ K}$ (Figure 6b).

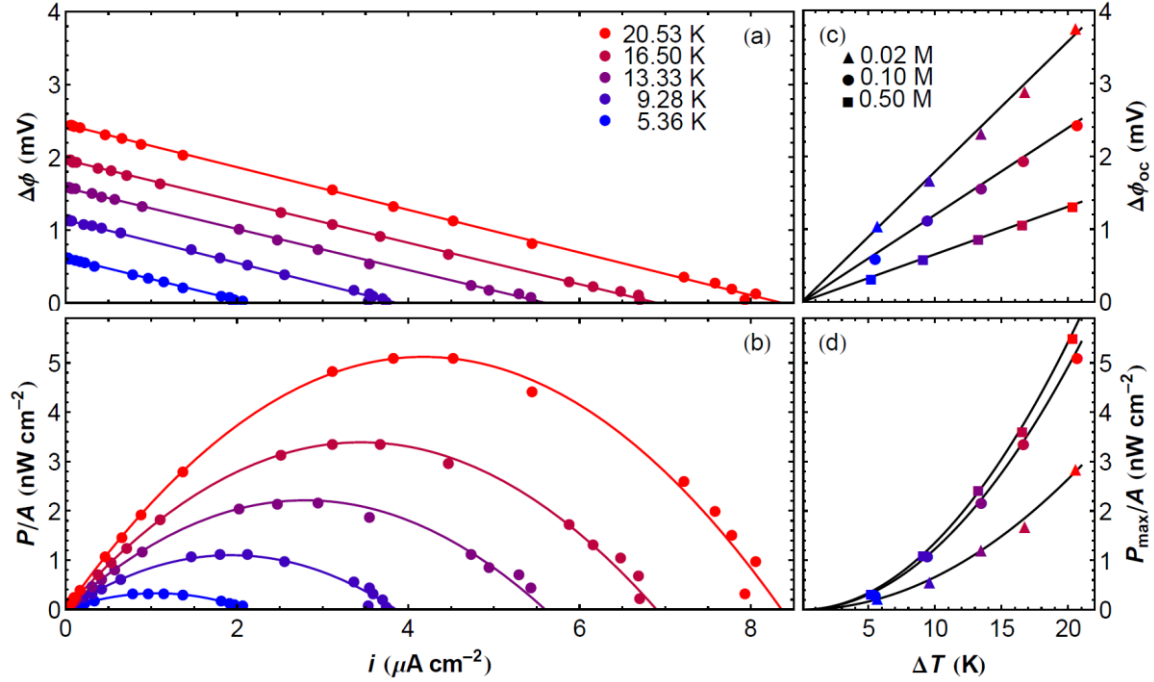


Figure 6. (a and b) Thermally-generated voltage $\Delta\phi$ and power output P/A in 0.10 mol/L NaCl solutions vs. electric current density through the external load for different ΔT . The practically identical slopes of the $\Delta\phi-i$ curves indicate that R_{int} is independent of ΔT . The power output is parabolic in the current density and its maximum value is $P_{\text{max}}/A = i_{\text{sc}}\Delta\phi_{\text{oc}}/4$, where $i_{\text{sc}} = \Delta\phi_{\text{oc}}/(AR_{\text{int}})$ is the short-circuit current density; P_{max}/A is given by the area of the largest rectangle under the $\Delta\phi-i$ curve. (c and d) Open-circuit thermally-generated voltage $\Delta\phi_{\text{oc}}$ and maximum power output P_{max}/A vs. the temperature difference.

Figure 6c shows that the open-circuit potential is proportional to the temperature difference ΔT between the solutions and that the Seebeck coefficient of the membrane thermocell (i.e. the slope) increases with decreasing electrolyte concentration, as observed in Figure 3a. The maximum power output is $P_{\text{max}} = I_{\text{sc}}\Delta\phi_{\text{oc}}/4 = (\Delta\phi_{\text{oc}})^2/4R_{\text{int}}$. Consequently, the maximum power output is

quadratic in the temperature difference, $P_{\max} \propto (\Delta T)^2$ (Figure 6d). This is an advantage over thermocells based on the temperature dependence of the electrode potential. The internal resistance of these cells shows a significant temperature dependence, and their complicated discharge behavior makes it difficult the prediction of the maximum power output [49].

4.5 The effect of the electrolyte concentration on the power output

The effect of the electrolyte concentration observed experimentally agrees with the predictions of eq 30. The experimental results in Figure 7a show the variation of the absolute Seebeck coefficient of the cell $\Delta\phi_{\text{oc}} / \Delta T$ with the NaCl concentration is approximately described by the function (solid line) $k(2R/F)\text{arcsinh}(X/2c)$ with $X \approx 3.0\text{mol/L}$. The internal electrical resistance of the cell R_{int} is inversely proportional to the electrolyte concentration c (Figure 7b). The variation of the maximum power output with the electrolyte concentration (Figure 7c) is the result of the concentration dependence of both $\Delta\phi_{\text{oc}} / \Delta T$ and R_{int} because $P_{\max} / (\Delta T)^2 = (\Delta\phi_{\text{oc}} / \Delta T)^2 / (4R_{\text{int}})$; note that $P_{\max} \propto (\Delta T)^2$ (Figure 6d). Thus, as observed in Figure 6d, there is a significant increase in power output when increasing the NaCl concentration from 0.02 mol/L to 0.10 mol/L, but only a minor increase when it is further increased to 0.50 mol/L.

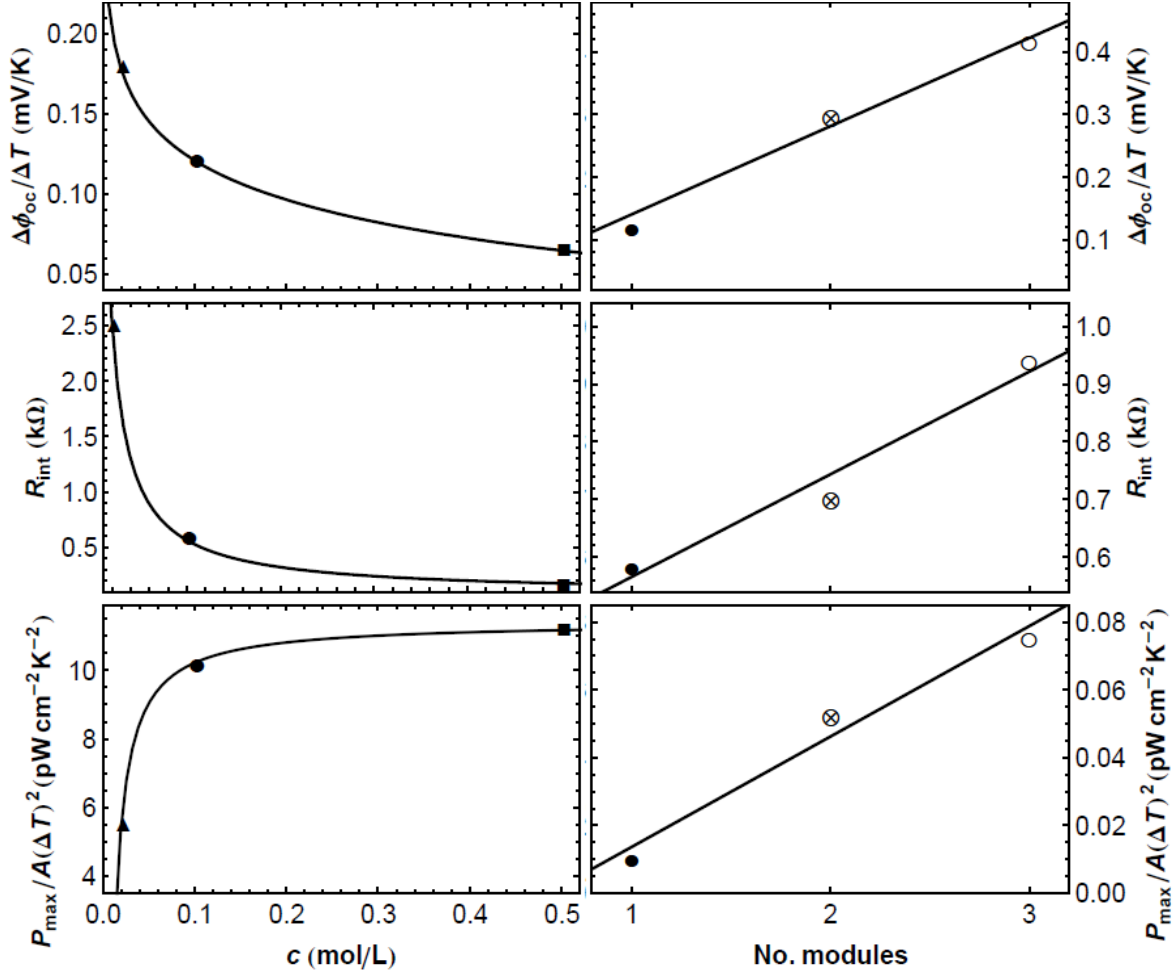


Figure 7. (a) The variation of the absolute Seebeck coefficient $\Delta\phi_{oc}/\Delta T$ with the NaCl concentration c is approximately described by the function $k(2R/F)\text{arcsinh}(X/2c)$ with $X \approx 3.0$ mol/L (solid line). (b) R_{int} is inversely proportional to c . (c) The maximum power output is $P_{max} = (\Delta\phi_{oc})^2/(4R_{int})$. The variation of $P_{max}/(\Delta T)^2 = (\Delta\phi_{oc}/\Delta T)^2/(4R_{int})$ with c is due to the concentration dependence of both $\Delta\phi_{oc}/\Delta T$ and R_{int} . (d) The Seebeck coefficient $\Delta\phi_{oc}/\Delta T$ for 0.1 mol/L NaCl increases linearly with the number of modules. The straight line passes through the origin. (e) R_{int} increases linearly with the number of modules (but the line has non-zero

intercept due to the electrode compartments). (f) The peak power density also increases with the number of modules.

4.6 The effect of the number of modules

Increasing the number of “hot solutions” and hence of anion- and cation-exchange membrane pairs in the cell increases the thermally-generated voltage and the maximum power output. The increase in $\Delta\phi_{oc}$ is linear in the number of membrane pairs because the composed cell behaves as a battery of modules generating equal and additive thermal potentials (Figure 7d). The cell with one module has two electrode compartments and two solution compartments (hot and cold), separated by three ion-exchange membranes. A second module adds two solution compartments and two more membranes, and so on. Thus, the cell resistance R_{int} also increases with the number of modules (Figure 7e). The peak power density $P_{max} / A = (\Delta\phi_{oc})^2 / (4R_{int})$ also increases with the number of modules (Figure 7f) due to the dominant role of the increase in $\Delta\phi_{oc}$.

Figures 8a and 8b show the dependence of $\Delta\phi$ and the power output P/A with the output current through a variable external load for cells with 0.10 mol/L NaCl and one, two and three modules and temperature differences of around 16.5 K. Contrary to the case of Figure 6a where the $\Delta\phi-i$ lines were parallel because R_{int} is independent of ΔT , the $\Delta\phi-i$ lines in Figure 8a are not parallel because R_{int} varies with the number of modules. The thermally-generated voltage $\Delta\phi_{oc}$ is linear in ΔT and the maximum power output P_{max} / A is quadratic in ΔT (Figures 8c and 8d).

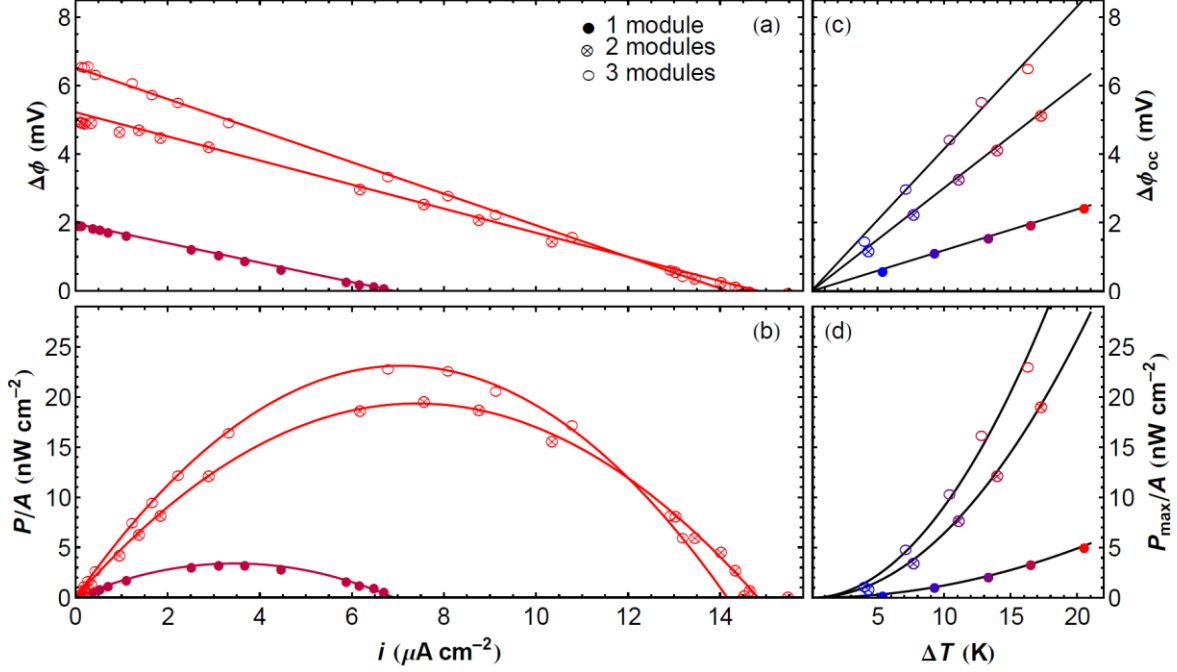


Figure 8. (a and b) Thermally-generated voltage $\Delta\phi$ and power output P/A vs. electric current density through a variable external load for cells with 0.10 mol/L NaCl and one, two and three modules and similar ΔT : 16.5 K (1 module), 17.3 K (2 modules), 16.3 K (3 modules). The different slopes of the characteristic $\Delta\phi-i$ curves indicate that R_{int} varies with the number of modules. The power output is parabolic in the current density and its maximum value is $P_{max}/A = (\Delta\phi_{oc})^2 / (4AR_{int})$. (c and d) Open-circuit voltage $\Delta\phi_{oc}$ and maximum power output P_{max}/A vs. ΔT for cells with 0.10 mol/L NaCl and one, two and three modules.

5. Discussion and conclusions

The Seebeck coefficients of different ion-exchange membrane systems in the absence of temperature difference between the electrodes have been measured in order to investigate the thermal membrane phenomena. The major contribution to the thermal membrane potential has been attributed to the non-isothermal Donnan potentials at the membrane interfaces. Using stacks

of anion- and cation-exchange membranes, the application of the thermal membrane potential to thermoelectric power generation has been demonstrated experimentally. Electrolytes with positive heat of transport have been found to decrease the generated potential. Therefore, electrolytes with small (or negative) heat of transport should be used to enhance the Seebeck coefficient.

Very good agreement between all the measurements and the theory presented in Section 2 has been observed. The measured Seebeck coefficients have presented a clear correlation with the heats of transport of different electrolytes; although KCl and KI have shown some deviation. The largest Seebeck coefficient in 0.02 mol/L concentration has been observed with KI. Among the chlorides, the ordered series KCl, LiCl, NaCl, TMAcI, and HCl exhibits a descending Seebeck coefficient (Figure 4). This result is in agreement with previous observations. Hanaoka et al. [17] obtained the same descending order of Seebeck coefficients for cation-exchange membranes and a concentration range 1–100 mmol/L. By contrast, Barragán and Ruiz-Bauzá [18] reported a descending Seebeck coefficient order of LiCl, NaCl and KCl in 1 mmol/L concentrations, and explained their results by the increasing molar mass of the cation and did not comment on the ionic heats of transport. Kiyono et al. [16] reported that the order can vary depending on the membrane ion-exchange capacity, water uptake, and electrolyte concentration, but KCl always exhibited a Seebeck coefficient larger than that of NaCl. Our results have suggested that the heat of transport inside the membranes is different to that in the aqueous phase, which might also explain the different behaviours observed by different authors. In addition, some theoretical simplifications, such as neglecting the water thermo-osmosis, should be critically considered.

With the proposed cell design, it has been shown that electrical power can be generated from waste heat (i.e., from temperature differences). Due to the linear dependence of the thermal membrane potential on the temperature difference, $\Delta\phi \propto \Delta T$, the power output has been observed

to scale with the temperature difference squared. The Seebeck coefficient can be increased by selecting electrolytes with low or negative heat of transport, which should also increase the power, assuming that the conductivity does not decrease. Figure 7 has demonstrated that a higher electrical conductivity of the membrane system is paramount to draw any meaningful power from the thermocell. We have shown that an increase of the electrolyte concentration beyond 0.1 mol/L produces no significant increase in the maximum power because, even though it decreases the total resistance of the cell, it also decreases the Seebeck coefficient. With more membranes in series, the linear increase in the Seebeck coefficient and the thermal potential with the number of modules has led to a power increase, although not scaled with the square of the number of modules because of the reduction in the total conductivity of the cell.

The power produced by the system with NaCl is obviously low, not to mention the expected efficiency. However, it is of the same order of magnitude than obtained with other emerging thermoelectric technologies, such as organic thermoelectrics [50]. Furthermore, some improvements in performance are possible by further optimizing the cell and the electrolyte. The effective temperature difference across the membrane is only about one third of the applied temperature difference. As the thermal conductivity of the membranes is close to that of water, the magnitude of parameter k in eq 30 suggests that the temperature polarization layers are of the same thickness as the membranes. With enhanced mixing, the parameter k could be increased to a value of 0.9, which leads to a three-fold increase of the Seebeck coefficient. This could be realized by increasing the pumping speed of the solutions and directing the inlets towards the membranes, as is sometimes done (see e.g. Ref. [15]). If the cell resistance could be simultaneously decreased by 60%, by decreasing the distance between the electrodes and using highly conductive membranes, the maximum power would show an increase of approximately three orders of magnitude at 0.10

mol/L. Increasing the membrane charge density also increases the Seebeck coefficient as dictated by eq 30, and thus enables the use of more concentrated electrolyte solutions. The efficiency of the system could be further enhanced by decreasing the thermal conductivity of the membranes. However, even with the hypothesized performance, the power required for the (enhanced) mixing is likely to be much larger than the harvested power. Therefore, it would be logical to combine the system with processes where pumping effluents of above-ambient temperature is already required, e.g. cooling water of power plants. Also, geothermal resources such as hot springs and geysers are a possibility. Although applications of waste heat harvesting seem presently unrealistic, our experimental and theoretical results provide interesting physical insights into thermoelectric phenomena in ion-exchange membranes which are important across a range of membrane applications.

Supporting Information

Theoretical analysis of the potentiometric measurements of the counterion transport number.

AUTHOR INFORMATION

Corresponding Author

* lasse.murtomaki@aalto.fi

Tel. +358 50 570 6352

† Deceased September 29th, 2015. Prof. Kontturi participated in the revision.

Funding Sources

Funding from Aalto Energy Efficiency Research Programme is gratefully acknowledged. J. A. M. acknowledges the financial support from the Ministry of Economic Affairs and Competitiveness and the European Union (project MAT2012-32084), and the Generalitat Valenciana (project PROMETEO/2012/069).

ACKNOWLEDGMENTS

The help from Mr. Tuomas Vainikka, Mr. Jussi Nieminen and Mr. Martin Wiesing in building and testing the experimental setup is acknowledged.

REFERENCES

- [1] T.M. Tritt, Thermoelectric Phenomena, Materials, and Applications, *Ann. Rev. Mater. Res.*, 41 (2011) 433-448.
- [2] Q. Zhang, Y. Sun, W. Xu, and D. Zhu, Organic Thermoelectric Materials: Emerging Green Energy Materials Converting Heat to Electricity Directly and Efficiently, *Adv. Mater.*, 26 (2014) 6829-6851.
- [3] L.E. Bell, Cooling, Heating, Generating Power, and Recovering Waste Heat with Thermoelectric Systems, *Science*, 321 (2008) 1457-1461.
- [4] C. Xiao, Z. Li, K. Li, P. Huang, and Y. Xie, Decoupling Interrelated Parameters for Designing High Performance Thermoelectric Materials, *Acc. Chem. Res.*, 47 (2014) 1287-1295.
- [5] T.J. Abraham, D.R. MacFarlane, and J.M. Pringle, Seebeck coefficients in ionic liquids - prospects for thermo-electrochemical cells, *Chem. Commun.*, 47 (2011) 6260-6262.

- [6] O. Bubnova, X. Crispin, Towards polymer-based organic thermoelectric generators, *Energy Environ. Sci.*, 5 (2012) 9345-9362.
- [7] K.D. Sandbakk, A. Bentien, and S. Kjelstrup, Thermoelectric effects in ion conducting membranes and perspectives for thermoelectric energy conversion, *J. Membr. Sci.*, 434 (2013) 10-17.
- [8] T. Ikeda, Thermal Membrane Potential, *J. Chem. Phys.*, 28 (1958) 166-167.
- [9] M. Tasaka, S. Morita, and M. Nagasawa, Membrane Potential in Nonisothermal Systems, *J. Phys. Chem.*, 69 (1965) 4191-4197.
- [10] M. Tasaka, K. Hanaoka, Y. Kurosawa, and C. Wada, Thermal Membrane Potential Through Charged Membranes in Electrolyte Solutions, *Biophys. Chem.*, 3 (1975) 331-337.
- [11] R. Haase, *Thermodynamics of Irreversible Processes*, Dover, Mineola, N.Y., 1990.
- [12] M. Tasaka, R. Kiyono, and M.S. Huda, Membrane Phenomena in Nonisothermal Systems: Part 1. Theory, *Bull. Chem. Soc. Jpn.*, 70 (1997) 555-559.
- [13] M. Tasaka, N. Ichijo, S. Kobayashi, and H. Kobayashi, Thermal Membrane Potential Across Charged Membranes in NaCl - NH₄Cl and LiCl - NH₄Cl Solutions, *Biophys. Chem.*, 4 (1976) 269-274.
- [14] M. Tasaka, K. Ogawa, and T. Yamazaki, Thermal Membrane Potential across Charged Membranes in 2-1 and 1-2 Electrolyte Solutions, *Biophys. Chem.*, 7 (1978) 279-283.
- [15] K. Hanaoka, R. Kiyono, and M. Tasaka, Thermal membrane potential across anion-exchange membranes in KCl and KIO₃ solutions and the transported entropy of ions, *J. Membr. Sci.*, 82 (1993) 255-263.
- [16] R. Kiyono, O. Sekiguchi, and M. Tasaka, Thermal membrane potential across cation-exchange membranes for various halide solutions, *Colloid Polym. Sci.*, 271 (1993) 1183-1190.

- [17] K. Hanaoka, R. Kiyono, and M. Tasaka, Nonisothermal membrane phenomena across perfluorosulfonic acid-type membranes, *Flemion S: Part II. Thermal membrane potential and transported entropy of ions*, *Colloid Polym. Sci.*, 272 (1994) 979-985.
- [18] V.M. Barragán, C. Ruiz-Bauzá, Effect of unstirred solution layers on the thermal membrane potential through cation-exchange membranes, *J. Membr. Sci.*, 125 (1997) 219-229.
- [19] V.M. Barragán, C. Ruiz-Bauzá. On the dependence of the thermal membrane potential across cation-exchange membranes on the mean temperature, *J. Membr. Sci.*, 134 (1997) 75-84.
- [20] M.S. Huda, R. Kiyono, M. Tasaka, T. Yamaguchi, and T. Sata, Thermal membrane potential across anion-exchange membranes with different benzyltrialkylammonium groups, *Sep. Purif. Technol.*, 14 (1998) 95-106.
- [21] P.N. Snowdon, J.C.R. Turner, The concentration dependence of the Soret effect, *Trans. Faraday Soc.*, 56 (1960) 1812-1819.
- [22] J.N. Agar, C.Y. Mou, and J.L. Lin, Single-ion heat of transport in electrolyte solutions: a hydrodynamic theory, *J.Phys.Chem.*, 93 (1989) 2079-2082.
- [23] P.N. Snowdon, J.C.R. Turner, The Soret effect in some 0.01 normal aqueous electrolytes, *Trans. Faraday Soc.*, 56 (1960) 1409-1418.
- [24] V.A. Bui, L.T.T. Vu, and M.H. Nguyen, Modelling the simultaneous heat and mass transfer of direct contact membrane distillation in hollow fibre modules, *J. Membr. Sci.*, 353 (2010) 85-93.
- [25] F. Bellucci, Temperature polarization effects in thermo-osmosis, *J. Membr. Sci.*, 9 (1981) 285-301.

- [26] J. M. Ortiz de Zarate, F. Garcia-Lopez, and J.I. Mengual, Temperature polarization in non-isothermal mass transport through membranes, *J. Chem. Soc., Faraday Trans.*, 86 (1990) 2891-2896.
- [27] R. Skorpa, M. Voldsund, M. Takla, S.K. Schnell, D. Bedeaux, and S. Kjelstrup, Assessing the coupled heat and mass transport of hydrogen through a palladium membrane, *J. Membr. Sci.*, 394–395 (2012) 131-139.
- [28] K. Kontturi, L. Murtomäki, and J.A. Manzanares, *Ionic Transport Processes*, Oxford U. P., Oxford, 2014.
- [29] S. Kim, M.M. Mench, Investigation of temperature-driven water transport in polymer electrolyte fuel cell: Thermo-osmosis in membranes, *J. Membr. Sci.*, 328 (2009) 113-120.
- [30] S. Kjelstrup, D. Bedeaux, *Non-equilibrium Thermodynamics of Heterogeneous Systems*, World Scientific Publishing Co. Pte. Ltd., Singapore, 2008.
- [31] R.A. Robinson, R.H. Stokes, *Electrolyte Solutions: Second Edition (Revised)*, Butterworths, London, 1959.
- [32] J. Chanu, Thermal Diffusion of Halides in Aqueous Solution, in: *Advances in Chemical Physics*, John Wiley & Sons, Inc., Hoboken, NJ, 1967, pp. 349-367.
- [33] M.L.V. Ramires, Nieto de Castro, C. A., Y. Nagasaka, A. Nagashima, M.J. Assael, and W.A. Wakeham, Standard Reference Data for the Thermal Conductivity of Liquids, *JPCRD*, 24 (1995) 1377-1381.
- [34] M. Khandelwal, M.M. Mench, Direct measurement of through-plane thermal conductivity and contact resistance in fuel cell materials, *J. Power Sources*, 161 (2006) 1106-1115.
- [35] C.D. Price, Thermal diffusion in solutions of electrolytes, Tech Rep. U.S.A.F. Contract No. AF(052)-99 (AD0276280), (1961).

- [36] F. Römer, Z. Wang, S. Wiegand, and F. Bresme, Alkali Halide Solutions under Thermal Gradients: Soret Coefficients and Heat Transfer Mechanisms, *J. Phys. Chem. B*, 117 (2013) 8209-8222.
- [37] J. Chanu, Étude de l'effet Soret dans les solutions ioniques, *J. Chim. Phys.*, 55 (1958) 743-753.
- [38] D.G. Leaist, L. Hui, Conductometric determination of the Soret coefficients of a ternary mixed electrolyte. Reversed thermal diffusion of sodium chloride in aqueous sodium hydroxide solutions, *J. Phys. Chem.*, 94 (1990) 447-451.
- [39] J.N. Agar, J.C.R. Turner, Thermal Diffusion in Solutions of Electrolytes, *Proc. R. Soc. A*, 255 (1960) 307-330.
- [40] F.S. Gaeta, G. Perna, G. Scala, and F. Bellucci, Nonisothermal matter transport in sodium chloride and potassium chloride aqueous solutions. 1. Homogeneous system (thermal diffusion), *J. Phys. Chem.*, 86 (1982) 2967-2974.
- [41] N. Takeyama, K. Nakashima, Proportionality of intrinsic heat of transport to standard entropy of hydration for aqueous ions, *J. Solution Chem.* 17 (1988) 305-325.
- [42] N. Takeyama, K. Nakashima, A Reduction Rule in Heats of Transfer for Aqueous 1-1 Electrolytes, *J. Phys. Soc. Jpn.*, 52 (1983) 2692-2698.
- [43] T. Ikeda, Transported Entropies and Conventional Eastman Entropies of the Transfer of Some Univalent Ions in Aqueous Solutions at 25 °C, *Bull. Chem. Soc. Jpn.*, 37 (1964) 1485-1489.
- [44] C.J. Petit, M. Hwang, and J. Lin, Thermal diffusion of dilute aqueous NH_4Cl , Me_4NCl , Et_4NCl , $n\text{-Pr}_4\text{NCl}$, and $n\text{-Bu}_4\text{NCl}$ solutions at 25 °C, *J. Solution Chem.*, 17 (1988) 1-13.
- [45] J. Lin, J. Bierlein, and J. Becsey, Molar heats of transport of dilute aqueous HCl solutions: A potentiometric study, *J. Solution Chem.*, 3 (1974) 827-836.

- [46] K.F. Alexander, Zur Theorie der Thermodiffusion in Flüssigkeiten, Z. phys. Chem. (Leipzig), 203 (1954) 213-227.
- [47] J. Colombani, J. Bert, and J. Dupuy-Philon, Thermal diffusion in (LiCl, RH₂O), J. Chem. Phys., 110 (1999) 8622-8627.
- [48] C.J. Petit, K.E. Renner, and J.L. Lin, The entropy of transport of NaCl and KCl at 30 °C, J. Phys. Chem., 88 (1984) 2435-2436.
- [49] T.J. Kang, S. Fang, M.E. Kozlov, C.S. Haines, N. Li, Y.H. Kim, et al., Electrical Power From Nanotube and Graphene Electrochemical Thermal Energy Harvesters, Adv. Funct. Mater., 22 (2012) 477-489.
- [50] O. Bubnova, Z.U. Khan, A. Malti, S. Braun, M. Fahlman, M. Berggren, et al., Optimization of the thermoelectric figure of merit in the conducting polymer poly(3,4-ethylenedioxythiophene), Nat. Mater., 10 (2011) 429-433.